Earth Observation and Geomatics Engineering 6(1) (2022) 135-149

EARTH OBSERVATION AND GEOMATICS ENGINEERING

website: https://eoge.ut.ac.ir

# Investigation Impact of Massive Dust Storm on Aerosol Optical, Physical, Radiative Properties over Southwest Iran

**Eslam Javadnia [1] *, Negar Zahedi [2]**

[1]Department of Surveying Engineering, Faculty of Engineering, University of Zanjan, Zanjan, Iran
[2]School of Surveying and Geospatial Engineering, College of Engineering, University of Tehran, Tehran, Iran
[2]Department of Surveying Engineering, Faculty of Engineering, University of Zanjan, Zanjan, Iran

**Article history:**
Received: 2022-03-24, Received in revised form: 2022-4-11, Accepted: 2022-5-22

## ABSTRACT

In this paper, a variety of satellite data and ground measurements were used to provide a comprehensive analysis of the characteristics of two powerful dust storms that occurred over the southwestern parts of Iran in mid-March 2012 (first ~11-14 March and second ~15-18 March). In order to better understand the effects of these kinds of dust storms on aerosol optical and radiative properties different types of data were used during study days. The purpose of this study is an attempt to understand and analyze the effects of these kinds of dust storms on aerosol optical and radiative properties, and their sources origins using different types of data such as satellite observations, ground measurements, and model output. The analysis of dust aerosol characteristics based on the meteorological data collected in the city of Ahvaz, measurements of the closest AERONET site at Kuwait University, and satellite data from Moderate Resolution Imaging Spectroradiometer (MODIS), Ozone Monitoring Instrument (OMI), and the Cloud-Aerosol Lidar and Infrared Pathfinder Satellite Observation (CALIPSO) showed significant changes during dusty days compared to non-dusty days. During the two storms, horizontal visibility, temperature, and humidity of the area decreased significantly, reaching as low as 300 m, 12°C, and 23% on the day with the highest aerosol pollution (March 18). Also, during the dust storms, the AERONET aerosol optical depth (AOD) observations at the Kuwait University and the measured PM10 concentration in Ahvaz meteorological station increased by respectively 4.5 and 9 times, reaching as high as 2.7 and 2600 µg/m$^3$ on March 18. The high values of MODIS AOD and OMI aerosol index clearly showed the spatial growth of the storms, which affected the study area as well as many other countries around the Persian Gulf. The CALIPSO vertical profile of total attenuated backscatter at 532 nm showed the vertical expansion of the storm to an altitude of 6 km which confirms the high aerosol loading over the study region. The ARF values ranged between -63 to -16 w/m$^2$ (average: -39 w/m$^2$) at the top of the atmosphere, and between -202 to -83 w/m$^2$ (average: -132 w/m$^2$) at the bottom of the atmosphere. Such conditions can result in cooling at the surface and warming in the atmosphere. In addition, the results of the DREAM simulation showed good agreement with the retrievals from satellite observations, and also the analyses of the HYSPLIT model.

## KEYWORDS

Aerosol,
Dust Storm,
AERONET,
MODIS,
Meteorological parameters.

## 1. Introduction

Dust storms are common weather phenomena in arid and semi-arid parts of the Middle East. The Arabian Peninsula at the heart of this region is the third-largest source of dust in the world (Goudie & Middleton, 2001). It has been reported that southern Iraq and Kuwait have the highest number of

* Corresponding author

E-mail addresses: javadnia@znu.ac.ir (E.Javadnia)

dusty days in this area (Middleton, 1986). Iraq itself is one of the major sources of dust in the Middle East, greatly affecting the climate of its neighboring countries, especially Iran. In recent decades, the desertification of Syria and western Iraq and the natural and anthropogenic drying of Mesopotamian wetlands (between the Tigris and Euphrates) has turned these areas into major sources of dust for the entire Middle East region (Crook, 2009). The western parts of Iran, especially the southwestern cities of Ahvaz and Abadan, experience a significant number of dusty days because of their proximity to the large deserts of neighboring countries (Hamzeh et al., 2021). Most storms in this region occur in the spring and summer (Kutiel & Furman, 2003). According to the statistics of the Iran Meteorological Organization, over the last 50 years, the average number of dusty days in Ahvaz has been 68 per year (Shahsavani et al., 2012). It has been reported that dust storms increase the number of patients admitted to Ahvaz medical centers for respiratory problems by more than 70% and increase the mortality rate by 1.7% (Shahsavani et al., 2011).

Changes in the optical and physical properties of atmospheric aerosols during dust storms have long been a subject of interest to researchers. Depending on the type and characteristics of their dust particles, dust storms can lead to higher absorption or scattering of solar radiation and consequently warming or cooling of the terrestrial system (Alpert et al., 1998; Miller et al., 2004). To investigate the effect of dust on solar radiation at the top and bottom of the atmosphere, it is necessary to determine radiative forcing due to the presence of aerosols. In a study by Javadnia and Abkar (2017), they examined the radiation effect of dust storms by estimating the radiative forcing of the Middle East region during the dust storm of July 2009. Dust aerosols affect the climate system both directly by changing the Earth's radiation budget through scattering and absorption of solar radiation and indirectly by acting as cloud condensation nuclei (CCN), thereby changing both cloud albedo and lifetime (Bangert et al., 2013; Charlson & Heintzenberg, 1995). All of these processes may also alter the optical and physical properties and therefore the radiative properties of dust aerosols.

In mid-March 2012, two major dust storms hit the Middle East region. These storms were so large that they spanned thousands of kilometers from the Red Sea to Afghanistan and from the Arabian Peninsula to India (Aher et al., 2014; Alam et al., 2014; Basha et al., 2015; NASA Earth Observatory Natural Hazards, 2012). According to Gulf News, many meteorologists labeled these storms "super sandstorms". The present study attempted to further investigate the characteristics, sources, and effects of two of these storms in southwestern Iran (city of Ahvaz). This investigation was performed by the use of the data collected by the meteorological station of Ahvaz and the AERONET (AErosol RObotic NETwork) measurements at Kuwait University, which is the closest AERONET site to the study area. Over the years, there have been many studies on the dust events of the Middle East based on ground measurements and satellite data to better understand dust storms and their origins (Alam et al., 2014; Basha et al., 2015; Papi et al., 2022; Prakash et al., 2014; Smirnov et al., 2002; Soleimany et al., 2022). However, only a few of these studies have simultaneously used various types of ground data, satellite observations, atmospheric models, and back-trajectory analyses for accurate storm analysis.

In the present study, AERONET data were used to investigate the physical, optical and radiative effects of aerosols, meteorological data were used to examine the effect of storms on meteorological parameters, Moderate Resolution Imaging Spectroradiometer (MODIS) and Ozone Monitoring Instrument (OMI) data were used for Spatio-temporal storm tracking and the identification of main dust sources, and the Cloud-Aerosol Lidar and Infrared Pathfinder Satellite Observation (CALIPSO) were used to study the vertical distribution of aerosols in the atmosphere. Also, the Hybrid Single Particle Lagrangian Integrated Trajectory (HYSPLIT) model and the images from Dust Regional Atmospheric Model (DREAM) model simulation were used to investigate the pathways and possible source regions for the dust storm events and to simulate the dust concentration during the storms, respectively.

## 2. Study Area and Used Data

Because of its arid climate, southwestern Iran is one of the main sources of dust in the Middle East, along with Iraq, Kuwait, and the Arabian Peninsula (Kutiel & Furman, 2003). Figure 1-a shows a true color composite map of the Middle East. The green box indicates the study area. The region of interest in the current study including the location of the meteorological station of Ahvaz and the Kuwait University AERONET site is shown in Figure 1-b. Ahvaz is one of the most populous cities in southwestern Iran. This city is located about 150 km away from the northern coast of the Persian Gulf and has an average elevation of 18 m (above sea level). The average annual temperature and rainfall in Ahvaz are 32°C and 156 mm, respectively. Ahvaz and other cities in western and southwestern Iran are hit by dust storms every year in late winter, spring, and early summer (Broomandi et al., 2017; Maleki et al., 2016; Velayatzadeh, 2020). The meteorological data required for the investigations were collected from the meteorological station of Ahvaz located at 31°18′ N, 48°42′ E. This study also used the data of the Kuwait University AERONET site, which is the nearest AERONET site to southwestern Iran, to investigate the physical, optical and radiative effects of dust aerosols in the region. The sun photometer of this site is located in the Khalidiya campus of Kuwait University (29°18′ N, 47°53′

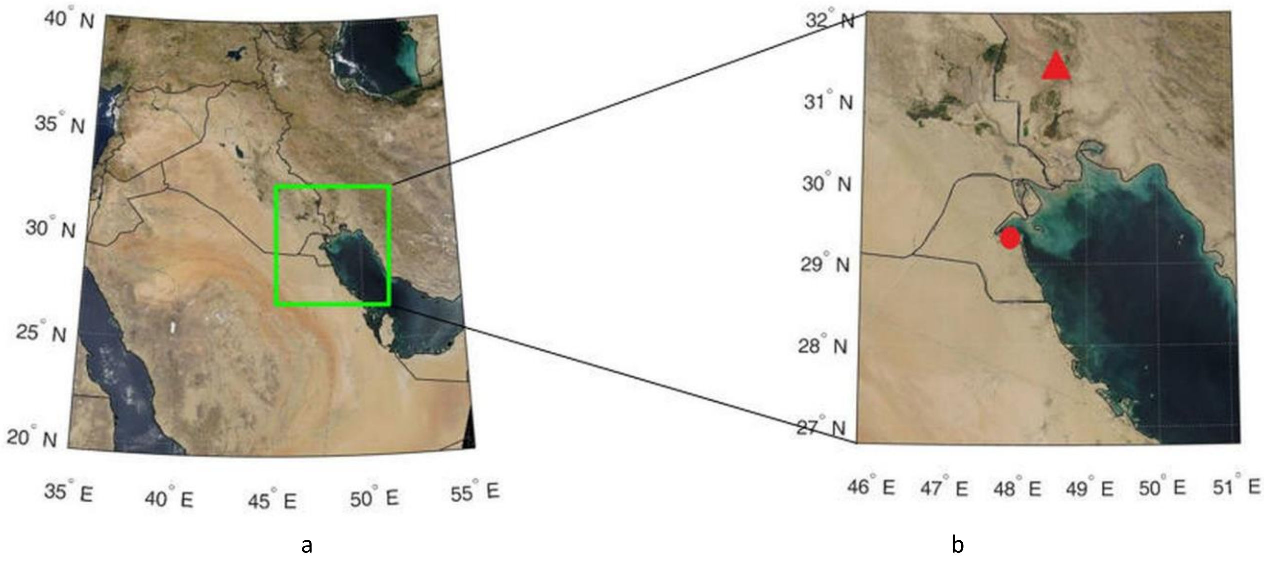


**Figure 1**. (a) true color composite map of the Middle East region (obtained from www.worldview.earthdata.nasa.gov) with the green box marking the study area; (b) true color composite map of the study area including the meteorological station of Ahvaz (red triangle) and Kuwait University AERONET site (red circle)

E), which is an urban area about 10 km out of Kuwait City. Kuwait, like Ahvaz, has a hot and dry climate.

### 2.1. Data and Models

#### 2.1.1. Meteorological Data

Meteorological data reported by the meteorological station of Ahvaz, which included horizontal visibility, temperature, relative humidity, and wind speed in 3-hour steps, were downloaded from the website of the Iran meteorological station (www.weather.ir). Particulate matter PM10 concentration data were obtained from the website of the department of environment of Khuzestan Province (www.doe.ir). All meteorological data and PM10 concentration data were collected for the period of March 3 to March 26, 2012.

#### 2.1.2. AERONET Data

One of the most common yet accurate ground-based methods for examining optical and radiative properties of aerosols is to use AERONET data provided by NASA (https://aeronet.gsfc.nasa.gov/). The CIMEL sun-photometer used in the AERONET network measures the direct sun radiance every 15 minutes in multiple channels (340, 380, 440, 500, 675, 870, 1020, and 1640 nm) (Holben et al., 1998). Then, the optical depth is computed based on the extinction of direct beam radiance at different wavelengths according to the Bouguer-Beer-Lambert law, which is called the direct method. Also, AOD is obtained by correcting optical depth for attenuation due to Rayleigh scattering and absorption by ozone and gaseous pollutants.

The sun-photometer also measures diffuse sky radiance at four wavelengths of 440, 670, 870, and 1020 nm. This parameter is used to retrieve aerosol volume size distribution, phase function, and single-scattering albedo (Dubovik & King, 2000; Holben et al., 1998). The procedure used to compute these parameters is known as the inversion method. The present study used level-1.5 version 2.0 AOD data, single-scattering albedo data, aerosol volume size distribution data, and Aerosol Radiative Forcing (ARF) data of Kuwait University AERONET site for the period of March 3 to March 17, 2012.

#### 2.1.3. OMI Data

OMI is onboard NASA's Earth Observing System (EOS) Aura satellite platform, which was launched in July 2004 (Levelt et al., 2006). OMI provides valuable information on aerosol absorption on a global scale in terms of the UV aerosol index (UV AI). The aerosol index is the difference between the measured radiances at 331 and 360 nm and the calculated radiances based on the radiative transfer theory for these wavelengths under pure molecular (Rayleigh particles) atmospheric conditions. This study used the daily AI data product in the form of a 1°×1° grid, which was obtained using the Giovanni tool of the NASA website (https://giovanni.gsfc.nasa.gov/).

#### 2.1.4. MODIS Data

MODIS instruments installed on the Terra and Aqua satellites, launched on December 1, 1999, and May 2, 2002, respectively. They provide good daily information on the characteristics of atmospheric aerosols. MODIS uses a Dark Target (DT) aerosol retrieval algorithm to produce MODIS standard AOD product using the data collected at near-infrared (2.1 and 3.8 µm) wavelengths (Kaufman et al., 1997).This product provides good information about the distribution of aerosols in different parts of the world, but it does not offer accurate estimates for bright surfaces such as deserts. The Deep Blue (DB) algorithm is more suitable for desert surfaces as it uses two bands of blue wavelength (0.412 and 0.470 µm) at which bright surfaces have lower reflectance compared to the 0.65 µm (Hsu et al., 2004). The present study used the daily level-3 MODIS aerosol product (MOD08-D3), which is produced by the combined application of DT and DB algorithms.

#### 2.1.5. CALIPSO Data

CALIPSO was launched on April 28, 2006, and offers valuable information on the properties of dust aerosols by measuring the vertical profiles of aerosols and clouds (Winker et al., 2006). CALIPSO has a 98° inclination orbit and flies at an altitude of 705 km, producing daily global maps of the vertical distribution of aerosols and clouds. It has three sensors onboard: Cloud-Aerosol Lidar with Orthogonal Polarization (CALIOP), Imaging Infrared Radiometer (IIR), and Wide Field Camera (WFC). CALIOP measures the profiles of the backscatter coefficient at 532 and 1054 nm and the linear depolarization profile at 532 nm. The depolarization measurements allow CALIOP to distinguish between ice and water clouds and also detect non-spherical aerosol particles (Sassen, 1991). CALIOP can detect and measure aerosols above bright surfaces under thin clouds as well as under clear sky conditions. This study used the level-4 CALIOP data including attenuated backscatter at 532 nm, depolarization ratio (DR) over 532 nm, vertical feature mask, and vertical profile of different aerosols. Since the CALIOP data of the study area for the entire period of interest (March 11 to March 18) were not available, only the data pertaining to March 20, 2012, were used.

#### 2.1.6. HYSPLIT Model

The Hybrid Single-Particle Lagrangian Integrated Trajectory (HYSPLIT) model is a commonly used tool for quantitative estimation of the source of dust-carrying air masses. The source of dust storms and the path that they traveled before reaching the study area can be investigated by using the HYSPLIT model to conduct a back-trajectory analysis, which means estimating the trajectories of air masses of interest a few days before the storm (Rolph et al., 2017). The meteorological data used in this model were derived from the datasets compiled by the NOAA Air Resources Laboratory. Since AOD represents the quantities of aerosols in the vertical column of the atmosphere, back-trajectory analysis is usually performed at three different altitude levels. In this study, the HYSPLIT model was used to analyze the trajectory of the storms of March 11 and March 15, 2012, three days before their arrival in the study area at three altitudes of 500, 1500, and 2500 m.

#### 2.1.7. DREAM Model

The Earth Sciences Department based at the Barcelona Supercomputer Center (BSC) has created a dust forecasting system called the Dust REgional Atmospheric Model (DREAM) (Basart et al., 2012; Nickovic et al., 2001). The new version of this model is called BSC- DREAM 8b. This model, which is a component added to the Eta/NCEP atmospheric model, predicts desert dust aerosols created by wind flows. In this study, this model was used to simulate surface dust concentration (in µg/m$^3$) in the study area during the dust storms of March 2012

## 3. Studied dust Storms

In mid-March 2012, two heavy dust storms hit the study area within the span of about 7 days (Figure 2a-Figure 2f). On March 11, the MODIS true color composite images and ground observations showed a huge amount of dust amassed on the border of Iran and Iraq, which seemed to be coming from the northwest and going into the study area and the Persian Gulf (Figure 2-a). According to the reports from the department of environment of Khuzestan Province (www.doe.ir) the dust mass observed on this day was so huge that in Ahvaz, dust concentration reached as high as 3700 µg/m$^3$ with a daily average of 1140 µg/m$^3$. On March 13, as the wind speed increased, Kuwaiti deserts added so much dust to the storm that the Kuwait University AERONET site recorded a peak aerosol optical depth (AOD) of 3 at 08:00 UTC and a daily average AOD of 1.6. According to observations made in Ahvaz and Kuwait, the storm subsided on March 14. As shown in Figure 2-d, on March 15, another dust storm entered the study area from the southwest (deserts of Saudi Arabia). On the last day of this storm in the region (March 18), as shown in Figure 2-f it was so strong that most flights in the Persian Gulf countries were canceled, schools were closed, and hospitals reported an influx of patients with respiratory problems. According to measurements made in Ahvaz on March 18, at 12:00UTC, dust concentration reached 4900 µg/m$^3$ (with a daily average of 2500 µg/m$^3$). In the following days, the storm moved out of the study area and into southern Iran and the Oman Sea. Ultimately, the storm reached Lahore on March 20, affecting large parts of Afghanistan and Pakistan on its path (Alam et al., 2014). The effects of the storm were also reported in western India on March 22 (Aher et al., 2014).

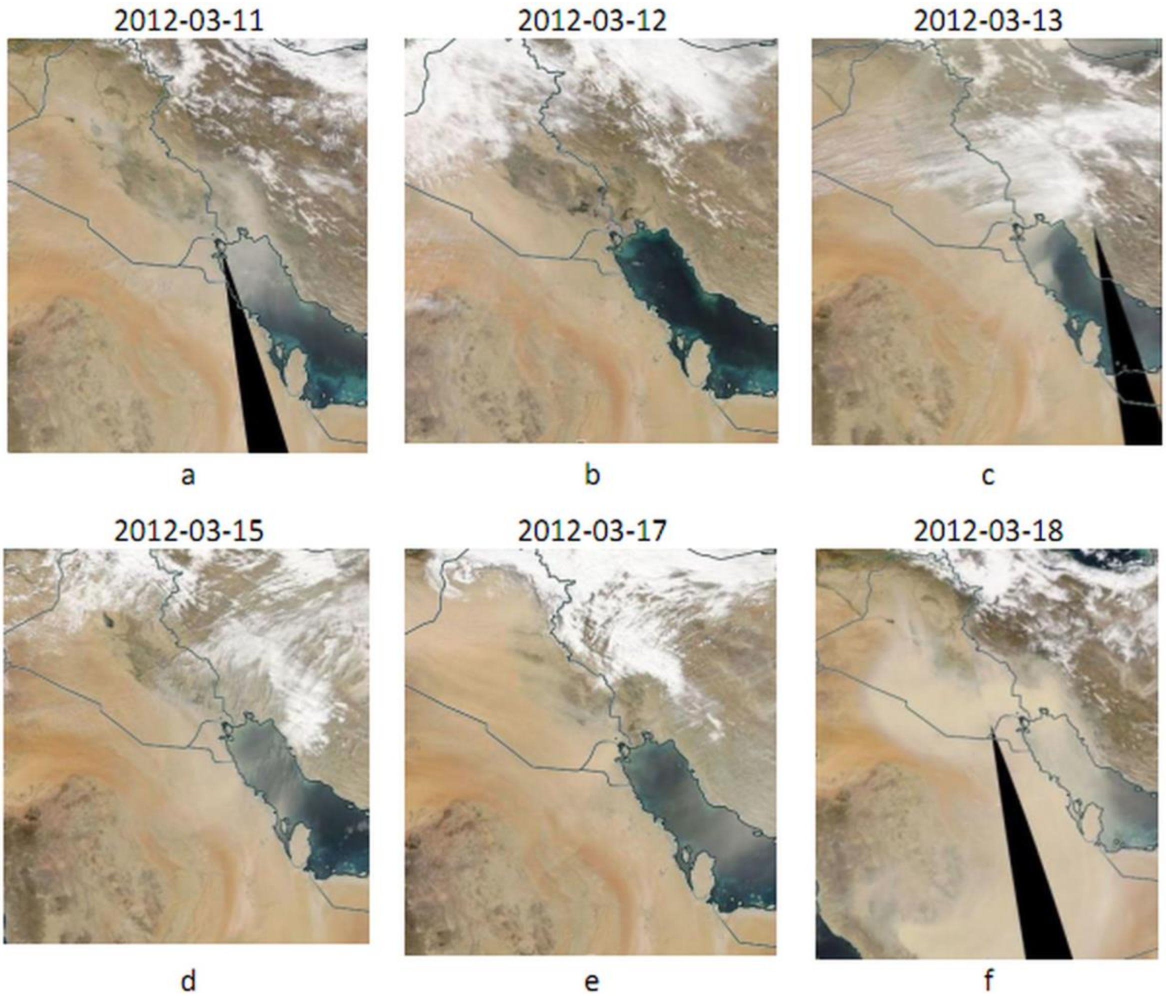


**Figure 2**. MODIS true color composite image of the first dust storm (March 11 to March 13, 2012) and the second dust storm (March 15 to March 18, 2012)

## 4. Results and Discussion

### 4.1. AOD and AI changes during the dust storms

According to the MODIS observations from March 11 to March 13, 2012 (the first storm) and from March 15 to March 18, 2012 (the second storm), the study sites (Ahvaz and Kuwait) had high AOD values in these periods. The spatial distribution of AOD values derived from MODIS data of March 13 and 18 (the peak days of the first and second storms, respectively) at 550nm is illustrated in Figure 3-a and Figure 3-b. The high AOD values at 550 nm clearly show the high aerosol load in the study area, which has led to reduced visibility and air quality and had adverse health effects. White areas in MODIS images indicate the places for which no data is available because of either cloud cover or algorithm limitations. The spatial average of AOD was computed using 9 × 9 pixels (~100 × 100 km per pixel) around each selected site. The average AOD in Ahvaz station and Kuwait site on March 13 and 18 was 1.2 and 1.5, respectively. The average AOD of these two sites from March 3 to March 26 was approximately 0.6.

Figure 4 (a-h) shows the regional distribution of aerosols according to the AI values obtained from OMI data three days before the peak of the first storm and three days before the peak of the second storm in the study area. AI values range from 1.5 to 3.3 for the first storm and from 1.7 to 3.8 for the second storm, indicating the spread of dust in the atmosphere of the study area. As shown in Figure 4 (a-d), for the first storm, dust formed on the border of Iraq and Syria on March 10, reached the study areas in the following days (March 11 to 13), and then grew toward the west and southwest of Iran. As Figure 4 (e-h) shows, for the second storm, dust formed in the deserts of Saudi Arabia on March 15, reached the study area in the following days, and then expanded to the Persian Gulf and the Southern parts of Iran. High AI values were observed during both storms. AI values on March 13 ($1.7<AI<3.0$) and on March 18 ($2.6<AI<3.8$), which were the peak of the storms, confirm the presence of dust with light-absorbing aerosols at the study sites (Ahvaz and Kuwait).

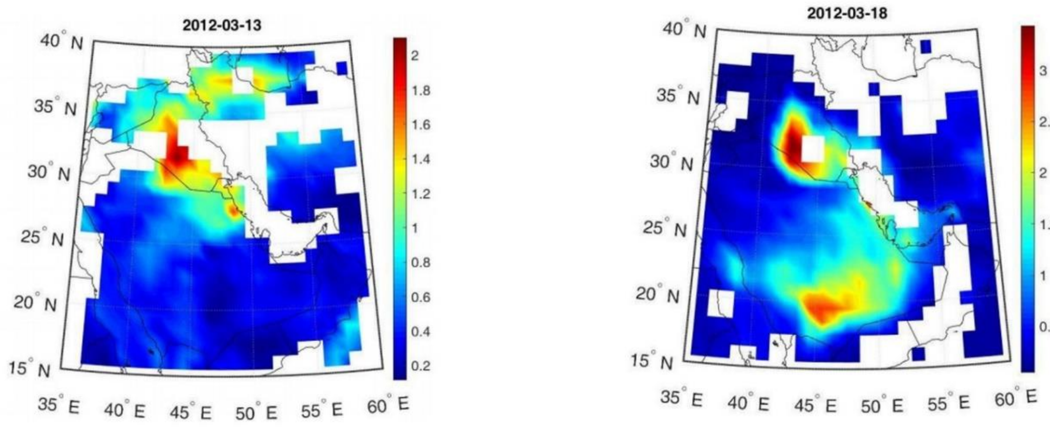


a b

**Figure 3**. Spatial distribution of aerosol optical depth (AOD) derived from MODIS data at 550 nm

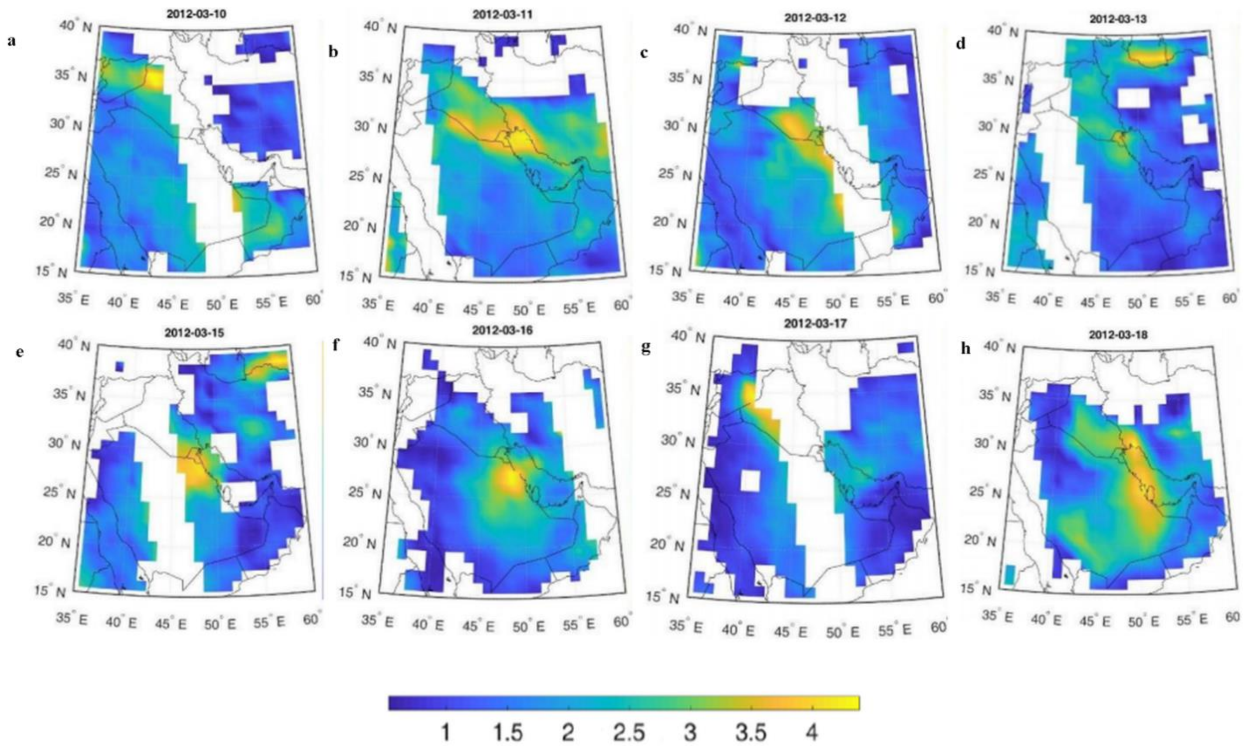


**Figure 4**. Map of UV-AI values derived from OMI data, showing the origin of the studied storms and their spread is in the study area

The HYSPLIT model was used to control and verify the results obtained from MODIS and OMI data regarding the source of dust-carrying air masses entering the study area. The Back-Trajectory analysis of the storm of March 11, 2012, from the site of Kuwait University (Figure 5-a), showed that the air masses reaching this area at altitudes of 500 and 1500 m had almost the same sources, which were Southeast Europe, the Mediterranean Sea, Turkey, Syria, and Iraq. Considering the time of collision of air masses coming from altitudes of 500 m and 1500 m, the main source of this storm is the Syrian-Iraqi border. The Back-Trajectory analysis carried out by the HYSPLIT model showed that the air mass of the dust storm of March 15, 2012 (Figure 5-b) at the altitude of 500 m originated in the Rub' al Khali desert in the southeast of Saudi Arabia and the Ad-Dahna desert in central Saudi Arabia. At the altitudes of 1500 m and 2500 m, the air masses of this storm came from the Red Sea and the border between the Ad-Dahna desert and the An-Nafud desert in northern Saudi Arabia.

In conclusion, according to MODIS and OMI observations and the HYSPLIT model, the main source of dust for the first storm of March 2012 (from March 11 to March 13) was the deserts of the Syrian-Iraqi border, but the dust of the second storm (from March 13 to March 18) mainly originated from the deserts of northeastern and eastern Saudi Arabia.

#### 4.2. Effect of Dust Storms on Meteorological Parameters in Ahvaz

The effects of the studied dust storms on meteorological parameters including PM10, horizontal visibility (HVIS), temperature, relative humidity, and wind speed in Ahvaz meteorological station from March 3 to March 26, 2012, were investigated (Figure 6-a to Figure 6-d). The daily average PM10 variation is illustrated in Figure 6-a. This figure shows two peak PM10 concentrations, 1100 µg/m$^3$ on March 11 and 2600 µg/m$^3$ on March 18, which coincide with the peak of two storms in the city of Ahvaz. The peak PM10 concentrations on March 11 and March 18, 2000 µg/m$^3$ and 5000 µg/m$^3$ occurred at 06:00 UTC (09:30 local time), respectively. The results showed that the average PM10 concentration on dusty days has been up to 9 times higher than the average value on non-dusty days. According to European Directive on air quality, exposure to PM10 concentrations of over 50 µg/m$^3$ for more than 35 days per year can be damaging to human health (Buchholz et al., 2011). This is while even the PM10 concentrations measured in Ahvaz on non-dusty days of March 2012 have been above 50 µg/m$^3$.

Figure 6-b shows the daily average horizontal visibility at Ahvaz meteorological station from March 3 to March 26, 2012. The average horizontal visibility decreased by about 13 km on non-dusty days of March 3 to 10, by 3 km on dusty days of March 11 to 14, and reached 2 km on dusty days of March 15 to 18. The lowest daily average horizontal visibility in Ahvaz was recorded on March 11 and 18, when horizontal visibility dropped below 500 m for 9 and 15 hours, respectively. The lowest horizontal visibility occurred on March 11 at 09:00 UTC (12:30 local time), with horizontal visibility dropping below 100 m (with a daily average of 2 km). On March 18, at 15:00 UTC (18:30 local time), horizontal visibility reached its lowest point in March at 50 m (with a daily average of approximately 300 m). In other words, during these hours, the dust storm reduced the horizontal visibility of Ahvaz by 130 and 260 times, respectively.

Figure 6-c shows the average daily temperature and relative humidity at Ahvaz Meteorological Station from March 3 to March 26, 2012. During the two days before the first storm, i.e. on March 9 and 10, the air temperature was 19.2 °C and 17.7 °C and the relative humidity was 36% and 33%, respectively. During the storm on March 11, the temperature and humidity dropped to 15.8 °C and 23%. In other words, during the peak of the first storm, the air temperature decreased by 10% and the relative humidity by 31% compared to the average of the previous two days. During the two days before the peak of the second storm, i.e. on March 16 and 17, the air temperature was 18.9 °C and 16.4 °C and the relative humidity was 46% and 38%, respectively. During the peak of this storm on March 18, the temperature reached its lowest point in March, i.e. 11.7 °C, and humidity dropped to 23% as in the previous storm. In other words, on the peak day of the second storm, the air temperature decreased by 27% and the relative humidity by 36% compared to the average of the previous two days. The temperature and humidity of the area stabilized and returned to normal in the days following the two storms.

Figure 6-d shows the daily average wind speed at Ahvaz Meteorological Station from 3 to 26 March 2012. In general, the wind speed on the day of the storms on March 11 and 18 was lower than on the preceding days.

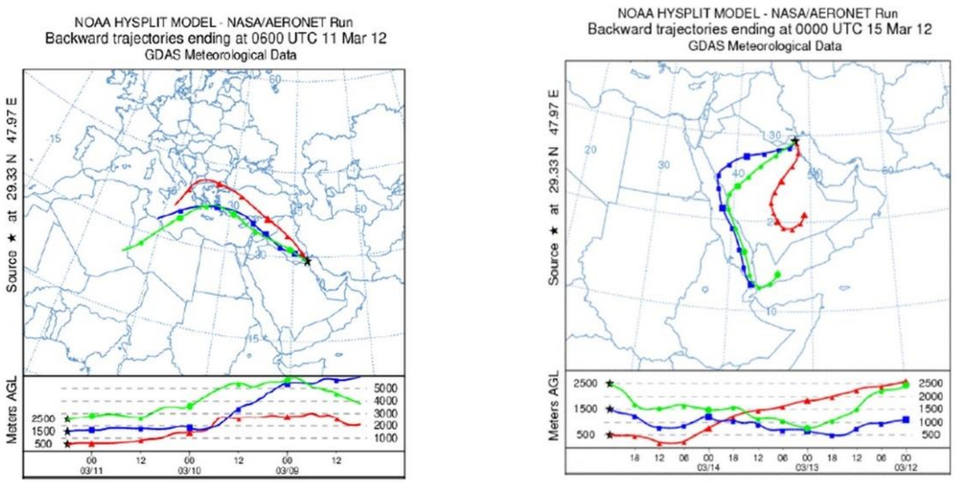


**Figure 5**. Back-Trajectory analysis of the storms of March 11 and 15, 2012 at different altitudes from the site of Kuwait University (conducted with HYSPLIT)

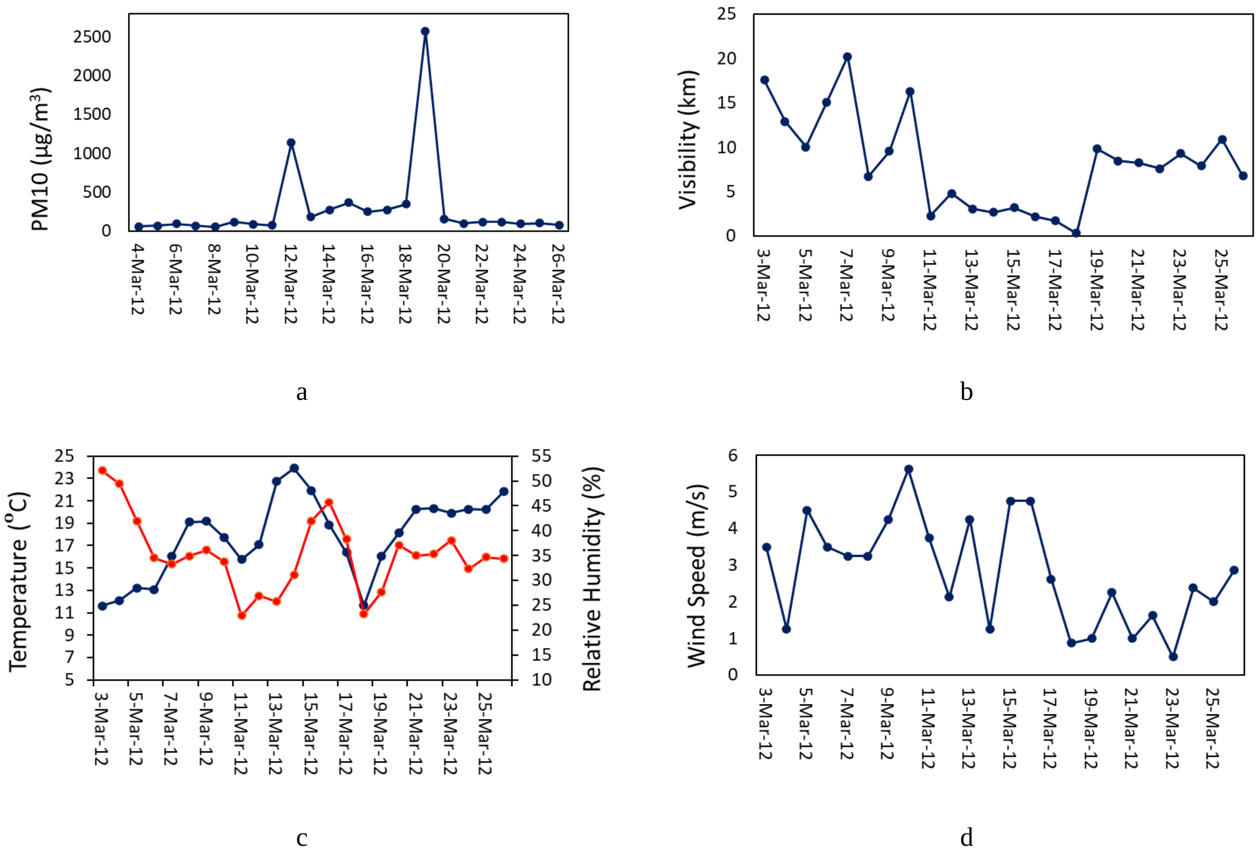


**Figure 6**. The daily averages variations of meteorological parameters including (a) PM10 concentration (µg/m$^3$), (b) horizontal visibility (km), (c) temperature (°C) and relative humidity (%), and (d) wind speed (m/s)

### 4.3. Optical Measurements of Aerosols

Figure 7 shows the daily variation in the AOD measurements of the sun-photometer, the AOD values derived from MODIS data, and the Angstrom exponent at the AERONET site of Kuwait University from March 3 to March 26, 2012. It should be noted that no measurements were made in the AERONET site in the period between March 19 and March 24. As shown in Figure 7, the AOD measurements made by the sun-photometer at 500 nm (green) ranged from 0.078 to 0.488 on non-dusty days (March 3 to 10) but significantly increased during dusty days, reaching 0.48 (min) and 1.62 (max) during the first storm (from March 10 to March 14) and to 0.55 (min) and 2.72 (max) during the second storm (March 15 to March 18). These measurements show that the average AOD values on the days of the first storm and the second storm were respectively 3.6 and 5.2 times the average AOD on non-dusty days. A similar trend was observed in the measurements made at 1020 nm (red) and 1460 nm (purple). Figure 7-a also shows the daily changes in the AOD values obtained from MODIS at 550 nm for the Kuwait University site from March 3 to 26, 2012 (black). Since MODIS data contained no measurement for the AERONET site for the period between March 19 to March 24, the AOD of these days was not derived from MODIS data. Similar to the AOD values extracted from the AERONET site, the AOD values obtained from MODIS data clearly showed two major peaks conceding with the two studied storms. These AOD values had an average of 0.85 ± 0.33 and 1.14 ± 0.47 on dusty days of March 11 and March 18 (the first and second storms) and an average of 0.38 ± 0.14 on non-dusty days. The average AOD values showed respectively 2.2 and 2.9- fold increase in the first and second dust event compared to non-dusty days.

In general, it can be stated that the two storms significantly increased not only aerosol concentration but also coarse-mode aerosol distribution. The dust aerosol size distribution was investigated by estimating the Angstrom exponent or α (an index for expressing aerosol particle size distribution). Many studies have reported on the utility of

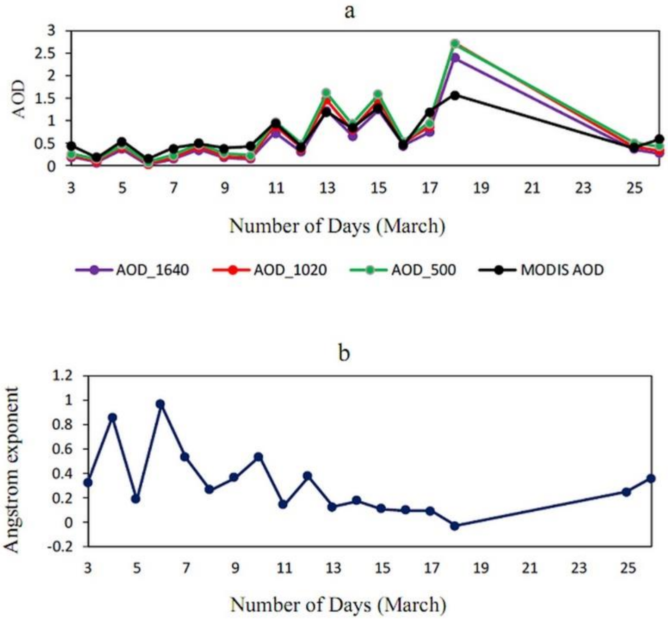


**Figure 7**. (a) Daily variation of AOD values derived from MODIS data at 550 nm (black) and the AOD measurements of the sun-photometer at wavelengths of 500 nm (green), 1020 nm (red), and 1640 nm (purple); (b) Daily variation of Angstrom exponent at the Kuwait University AERONET site from March 3 to March 26

this index in better understanding the size distribution of aerosols (Dumka et al., 2014; More et al., 2013; Wang et al., 2004). In general, if α is close to 2, it is indicative of the dominant presence of fine-mode aerosols, and if it is close to zero, it signifies the dominance of coarse-mode aerosols. In the present study, α of dusty days (Figure 7-b) was close to zero or negative, indicating the predominance of coarse-mode aerosols during storms. The average α of the area during the first and second storms was 0.20 and 0.06, respectively. This is while the average α of the area during non-dusty days was approximately 0.5. For example, on March 6, which was a clear day, α was close to one.

Figure 8 shows the variation of the single-scattering albedo (SSA) according to the measurements of Kuwait University AERONET at four wavelengths of 440, 675, 870, and 1020 nm on different days of March 2012, including March 3 to 10 (non-dusty days), March 11 to 14 (the first storm), and March 15 to 17 (the second storm). SSA is the ratio of the scattering to the total (scattering + absorption) extinction efficiency of aerosols. SSA can provide broad information on the absorption and scattering properties of aerosols (Dubovik et al., 2002). On the dusty days, SSA values were in the range of 0.86-0.98, which is abnormally high. The maximum SSA was 0.98 and occurred at a wavelength of 1020 nm. On both dusty and non-dusty days, SSA was higher at longer wavelengths, indicating that the scattering behavior and cross-section of aerosol particles increase with increasing wavelength. These results are comparable to the results of various other studies on dust storms in the Middle East and other regions (Alam et al., 2014; Basha et al., 2015).

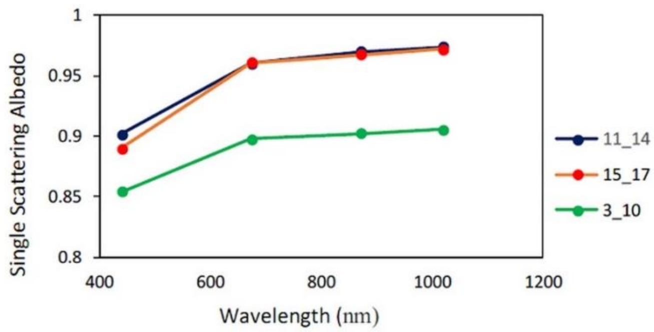


**Figure 8**. Spectral variation of single-scattering albedo obtained from the Kuwait University AERONET site in the periods before the storm (March 3 to 10), during the first storm (March 11 to 14), and during the second storm (March 15 to 17)

Figure 9 shows the aerosol volume size distribution (VSD) at the AERONET site from March 3 to March 30, 2012, which is partitioned into two groups of dusty days (March 11 to 14 for the first storm and March 15 to 17 for the second storm), and two groups of non-dusty days (March 3 to 10 for the period before the storm and March 25 to 30 for the period after the storm). VSD provides general information about coarse-mode (0.25-10 µm) and fine-mode (0.05-0.25 µm) aerosol contribution. A detailed description of the method of computing VSD and its accuracy can be found in the studies of Dubovik and King (2000). On average, the coarse-mode aerosol VSD on dusty days has been about 1.5 -times higher than on non-dusty days. To be more specific, coarse-mode aerosol VSD on March 13 and 15 (during the dust storms) has been 3-times higher than the corresponding values on non-dusty days. During a dust storm that hit the same area in July 2009, coarse-mode aerosol VSD was about 2 to 4 times higher as compared to non-dusty days (Javadnia & Abkar, 2017). Also, the spectral curve obtained for non-dusty days is smoother than the one for dusty days. The differences in the shape of these curves indicate that aerosols have had different properties (radii, compositions, etc.) during the period of interest. The maximum aerosol VSD for both storms was observed at a radius of 2.24. The height of the peak points for the first and second storms was 1.08 and 1.09, respectively. In the dust storm that occurred in the same area in July 2009, as in the present study, the maximum VSD occurred at a radius of 2.24 (Javadnia & Abkar, 2017).

reaching as low as -202 W/m$^2$. No data was available for March 18 (the peak of the second storm). In summary, the average ARF-BOA reached -126 W/m$^2$ during the first storm and -136 W/m$^2$ during the second storm. The average aerosol radiative forcing at the top of the atmosphere (ARF-TOA) was about -9 W/m$^2$ on non-dusty days (March 1 to 10), decreased to -33 W/m$^2$ on March 11, and then further dropped to -63 W/m$^2$ on March 13, and finally on March 15 reached -58 W/m$^2$, which indicates an increase in outgoing radiation because of the presence of heavy dust storms in the area. In summary, the average ARF-TOA reached -40 W/m$^2$ during the first storm and -38 W/m$^2$ during the second storm. Overall, ARF-TOA increased 4-fold during the storm. AF showed a similar trend, reaching as high as 135 W/m$^2$ and 140 W/m$^2$ on March 13 and 15, respectively. The ARF values obtained in this study are highly consistent with previous reports (Alam et al., 2014; Basha et al., 2015; Javadnia et al., 2017). The study carried out by Javadnia et al., (2017) on the dust storm of July 2009 reported that during this storm, the average ARF over four sites in the Middle East (Ahvaz, Persian Gulf, Al Basrah, Kuwait city) was -117 W/m$^2$. In the study conducted by Alam et al., (2014), ARF-BOA during the storm of March 2012 in Pakistan was reported to be -194 W/m$^2$, but in the present study, ARF-BOA at the Kuwait University AERONET site reached -198 W/m$^2$. The ARF reported by Basha et al., (2015) for the storm of March 2012 in the UAE region was –210 W/m$^2$.

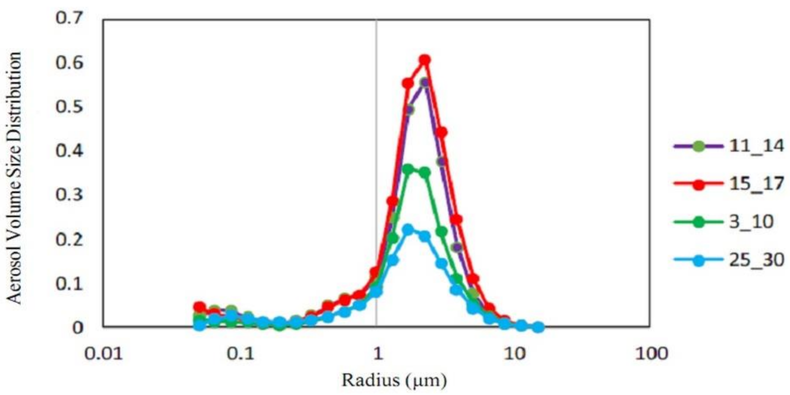


**Figure 9**. Variation of aerosol volume size distribution obtained from the Kuwait University AERONET site for March 2012 in two groups of dusty days (March 11 to 14 for the first storm and March 15 to 17 for the second storm) and two groups of non-dusty days (March 3 to 10 for the period before the storm and March 25 to 30 for the period after the storm)

### 4.4. Aerosol Radiative Forcing

As shown in Figure 10, the average aerosol radiative forcing at the bottom of the atmosphere (ARF-BOA) was about -50 W/m$^2$ during non-dusty days (March 3 to March 10), suddenly dropped to -104 W/m$^2$ with the arrival of the first storm on March 11, and dropped to its lowest point, -198 W/m$^2$, on March 13. With the arrival of the second storm on March 15, ARF-BOA again decreased significantly,

### 4.5. Vertical Dust Distribution

Despite their many merits, passive satellite sensors do not provide reliable estimates of aerosols over bright surfaces and are also susceptible to gaps in measurements because of the cloudiness of the atmosphere. In recent years, satellite-borne LIDAR systems are more commonly used to avoid such problems in the study and monitoring of aerosols. In this study, nighttime observations of CALIPSO were used to investigate the vertical dust distribution during the studied storms. The observations used for this purpose include the vertical profile of total attenuated backscatter at 532 nm, depolarization ratio, vertical feature mask, and aerosol subtype profile.

Figure 11-a shows the trajectory of CALIPSO on March 20, 2012. This study used the observations of this satellite on the blue part of this trajectory. The results are presented in Figure 11 (b-e). In this part of the study, the area of interest was the area within the coordinates 31.04°-18.85 N and 44.95°-47.95° E (dark box), which covers the sites of interest (Kuwait and Ahvaz) as well as a large part of Saudi Arabia from northeast to southwest (the trajectory of March 15 storm). The sites of interest (Kuwait and Ahvaz sites) are located on the left side of this frame, where data has some noise because of the presence of clouds in the area while the satellite was passing over it. Figure 11-b shows the profiles of total attenuated backscatter at 532 nm on March 20, 2012.

As can be seen, the study area has had a high level of backscatter, also extended to high altitudes of the atmosphere. The backscatter profile of CALIPSO for the study area shows a thick layer of dust that extends from the ground to a height of about 6 km. In Figure 11-c, this layer of dust is marked with yellow pixels. These results show that volume depolarization Ratio (DR) changes in the study area have been in the range of 0.2-0.3 in the altitude range of 2-4km. Volume DR is commonly used to study the vertical structure of dust layers. This parameter tends to be very high for irregularly shaped aerosols (non-spherical) such as dust, and close to zero for spherical particles such as cloud water droplets (Sassen, 1991). Figure 11-d shows the vertical feature mask obtained from CALIPSO data of the study area for March 20, 2012. This figure also clearly illustrates the presence of a significant layer of dust up to an elevation of 6 km (orange pixels). Because of the presence of a layer of cloud in the study area (turquoise pixels) from an altitude of 4 km to 8 km during the passage of CALIPSO over the sites of interest (Kuwait and Ahvaz), it has faced difficulty detecting dust in these sites. Figure 11-e shows the aerosol subtype profile obtained from CALIPSO data of the study area for March 20, 2012. This figure also clearly shows the presence of a dust storm in the area (yellow pixels with a very small number of brown pixels). In this image, yellow pixels represent dust and brown pixels represent pollution aerosols (a combination of fine-mode and coarse-mode aerosols).

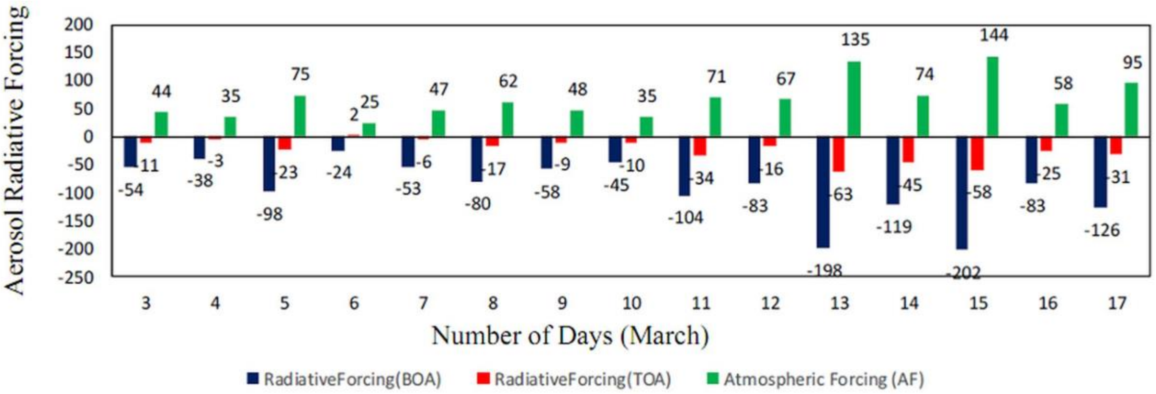


**Figure 10**. Aerosol radiative forcing in the study area (Kuwait University AERONET site) from March 3 to March 17, 2012

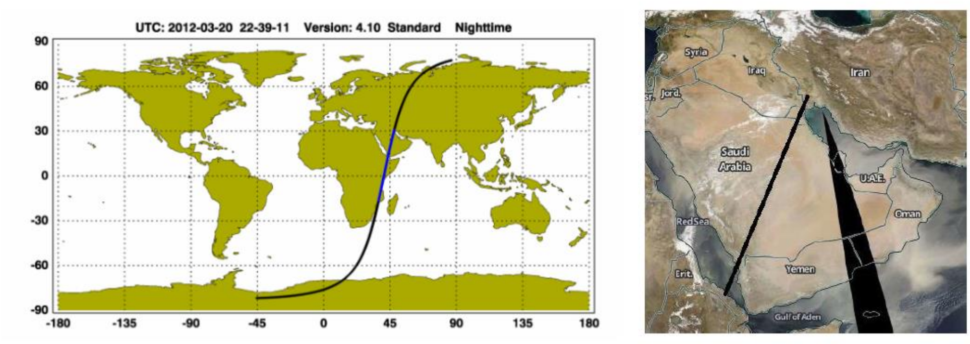


a

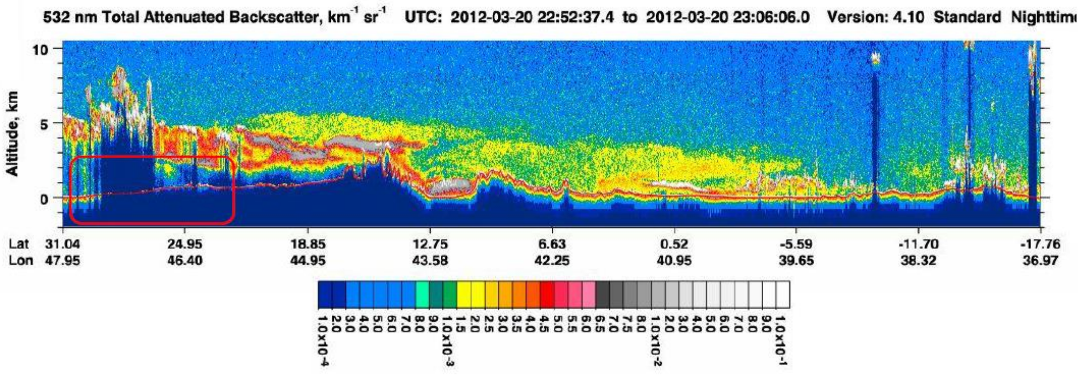


b

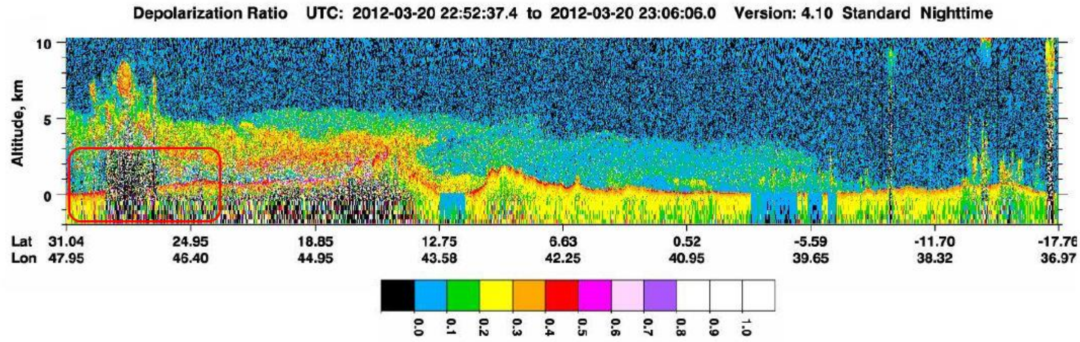


c

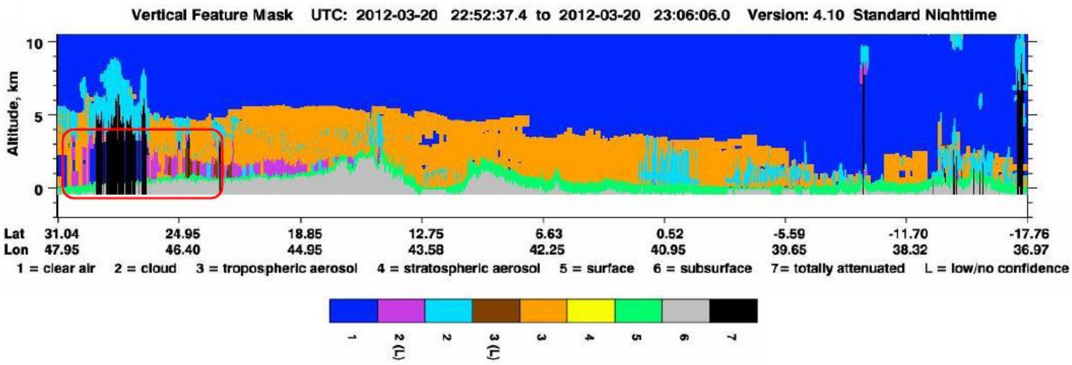


d

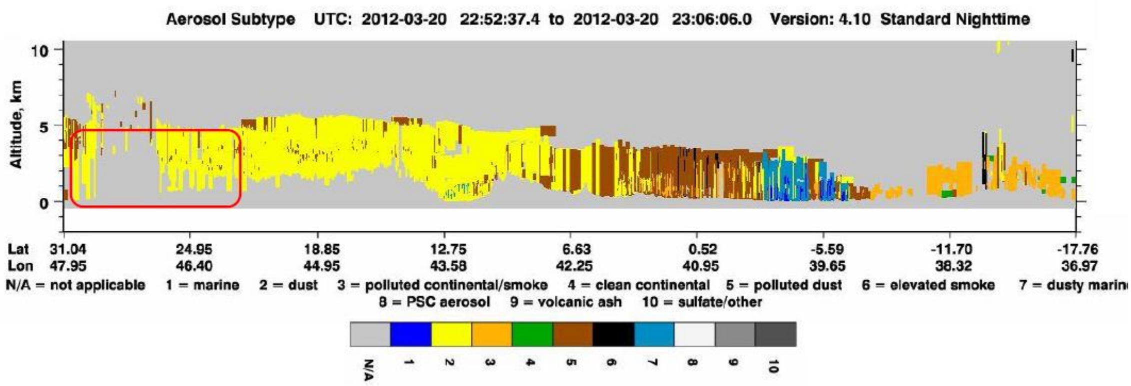


e

**Figure 11**. (a) The complete trajectory of CALIPSO and part of the trajectory for which data for March 20, 2012, were collected (blue); (b) part of the blue trajectory that covers the study area (black); (c) total attenuated backscatter at 532 nm; (d) depolarization ratio; (e) vertical feature mask; (f) aerosol type (red box is the domain of the trajectory marked in figure b)

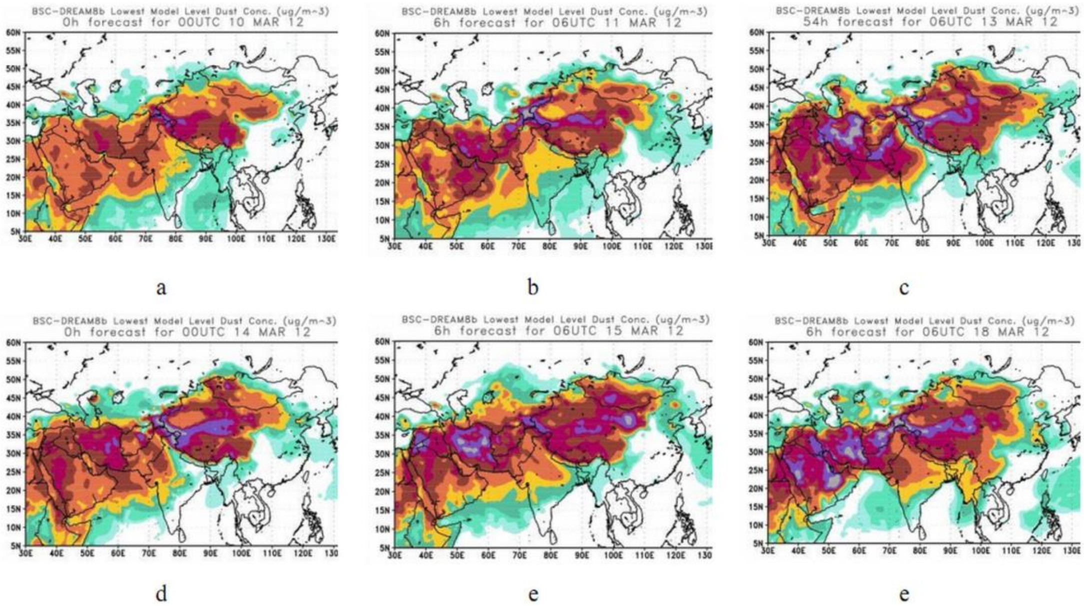


**Figure 12**. Surface dust concentration (in µg/m$^3$) obtained from the simulation of the storms of March 2012 in the study area with BSC-DREAM8b

#### 4.6. Storm Simulation with DREAM Model

BSC-DREAM8b was used to simulate to estimate surface dust concentration (in µg/m$^3$) in the study area during two dust storms. As shown in Figure 12-a to Figure 12-f, on March 10, which was a non-dusty day, dust concentration in the area was in the range of 160-320 µg/m$^3$. But this range changed to 320-640 µg/m$^3$ on March 11 and to 640-1280 µg/m$^3$ on March 13. On March 14, when the first storm moved out of the area, dust concentration returned to the normal level (like the level on March 10). On March 15, when the second storm began, dust concentration changed to 320-640 µg/m$^3$, and at the peak of this storm on March 18, it reached its highest level (1280-2650 µg/m$^3$). The spatial growth of the storm in the DREAM simulation showed that the first storm entered the Middle East from the Mediterranean coast and intensified in the deserts of Syria, Iraq, and northern Saudi Arabia before arriving at the study area. The second storm also entered the Middle East from the Mediterranean coast, but it intensified in the deserts of southern and southeastern Saudi Arabia before spreading throughout the region. The results of the DREAM simulation on the spatial distribution and source of the storms showed good agreement with the spatial distribution obtained from MODIS data, the regional distribution derived from OMI data, the vertical distribution observed by the LIDAR system of CALIPSO, and also the analyses made based on the HYSPLIT model.

Many parts of the Middle East, especially southwestern Iran, Iraq, Saudi Arabia, and the Persian Gulf, are among the places with the highest frequency of dust storms in the world. Studies on the dust storms of this region tend to be either lacking in terms of data diversity or use multiple types of data without detailed analyses. In the present work, two types of ground data, three types of satellite data, and two atmospheric models were used to study two major dust storms in this region as accurately as possible: a storm occurred in March 2012 which affected southwestern Iran for about 7 days (March 11 to 14), and a second more powerful storm, which affected the same area from March 15 to 18. The study was carried out by the use of ground data including local meteorological measurements and ground observations of the nearest AERONET site, satellite data including MODIS aerosol optical depth (AOD), OMI aerosol index, CALIPSO-retrieved aerosol vertical profiles, and atmospheric models including HYSPLIT and DREAM.

The results obtained by the analysis of MODIS and OMI data, which were confirmed by the results of the HYSPLIT model, showed that the main source of dust for the storm that lasted from March 11 to 13 was the deserts of the Syrian-Iraqi border, but for the second more powerful storm, which lasted from March 13 to March 18, the main dust source was the northeastern and eastern deserts of Saudi Arabia. Using the MODIS data of the study area (Ahvaz station and Kuwait site), the average AOD of the area on March 13 and March 18 was estimated to be 1.2 and 1.5, respectively, which indicates the high loading of aerosol in the region.

The analysis of meteorological data collected by Ahvaz meteorological station showed that March 18 was the day with the highest level of dust aerosol pollution in the entire period of the two storms. On this day, the average daily PM10 concentration was about 2600 µg/m$^3$ and this concentration reached as high as 5000 µg/m$^3$ at 06:00 UTC. The results showed that the average PM10 concentration in the dusty days of March 2012 was about 9 times that in non-dusty days. On March 18, horizontal visibility, temperature and humidity were 300 m, 11.7 °C, and 23% lower than the corresponding values on dusty days. For a few hours on this day, horizontal visibility even dropped below 100 m.

A summary of the main findings from this study is provided below.

- AOD observations of the Kuwait University AERONET site clearly showed two major peaks coinciding with the studied storms. During the first and second storms, the average AOD at this site increased significantly, reaching as high as, respectively, 3.6 and 5.2 times the average AOD on non-dusty days before these storms (March 3 to March 10).
- The Angstrom exponent (α) computed from the AERONET data was close to zero or negative on dusty days, indicating the predominance of coarse-mode aerosols during the storms. While the mean α on non-dusty days was about 0.5, it dropped to 0.20 during the first storm and to 0.06 during the second storm.
- Single-scattering albedo (SSA) values obtained from the AERONET data for dusty days were very high. The highest SSA 0.98 and obtained at a wavelength of 1020 nm.
- The volume size distribution (VSD) of aerosols during the dust storm was also derived from the AERONET data. Aerosol VSD on dusty days was on average 1.5-fold higher than that on non-dusty days.
- The ARF-BOA (aerosol radiative forcing at the bottom of the atmosphere) and ARF-TOA (aerosol radiative forcing at the top of the atmosphere) values computed based on the AERONET data for dusty days showed respectively 2-fold and 4-fold increase from before the storm. Such conditions can lead to lower temperatures in the bottom part of the atmosphere, cooling of the terrestrial system in areas affected by dust storms, and heating of the atmosphere.
- The aerosol vertical profile retrieved from the CALIPSO clearly showed the presence of a thick layer of dust in the study area, extending from the ground to an altitude of about 6 km, during the dust storms. The dust concentration results obtained from the simulation with DREAM model to investigate the source of dust and its spatial growth were highly consistent with the results obtained from other satellite data, demonstrating the utility of this model in the monitoring of dust movements in the study area.

**References**


Aher, G., Pawar, G., Gupta, P., & Devara, P. (2014). Effect of major dust storm on optical, physical, and radiative properties of aerosols over coastal and urban environments in Western India. International journal of remote sensing, 35(3), 871-903.

Alam, K., Trautmann, T., Blaschke, T., & Subhan, F. (2014). Changes in aerosol optical properties due to dust storms in the Middle East and Southwest Asia. Remote sensing of environment, 143, 216-227.

Alpert, P. a., Kaufman, Y., Shay-El, Y., Tanre, D., Da Silva, A., Schubert, S., & Joseph, J. (1998). Quantification of dust-forced heating of the lower troposphere. Nature, 395(6700), 367-370.

Bangert, M., Nenes, A., Vogel, B., Vogel, H., Barahona, D., Karydis, V., Kumar, P., Kottmeier, C., & Blahak, U. (2013). Saharan dust event impacts on cloud formation and radiation over Western Europe.

Basart, S., Pérez, C., Nickovic, S., Cuevas, E., & Baldasano, J. (2012). Development and evaluation of the BSC-DREAM8b dust regional model over Northern Africa, the Mediterranean and the Middle East. Tellus B: Chemical and Physical Meteorology, 64(1), 18539.

Basha, G., Phanikumar, D. V., Kumar, K. N., Ouarda, T. B., & Marpu, P. R. (2015). Investigation of aerosol optical, physical, and radiative characteristics of a severe dust storm observed over UAE. Remote Sensing of Environment, 169, 404-417.

Broomandi, P., Dabir, B., Bonakdarpour, B., & Rashidi, Y. (2017). Identification of the sources of dust storms in the City of Ahvaz by HYSPLIT. Pollution, 3(2), 341-348.

Buchholz, S., Krein, A., Junk, J., Gutleb, A. C., Pfister, L., & Hoffmann, L. (2011). Modeling, measuring, and characterizing airborne particles: case studies from southwestern Luxembourg. Critical reviews in environmental science and technology, 41(23), 2077-2096.

Charlson, R. J., & Heintzenberg, J. (1995). Aerosol forcing of climate. Wiley, Chichester.

Crook, J. (2009). Climate analysis and long range forecasting of dust storms in Iraq.

Dubovik, O., Holben, B., Eck, T. F., Smirnov, A., Kaufman, Y. J., King, M. D., Tanré, D., & Slutsker, I. (2002). Variability of absorption and optical properties of key aerosol types observed in worldwide locations. Journal of the atmospheric sciences, 59(3), 590-608.

Dubovik, O., & King, M. D. (2000). A flexible inversion algorithm for retrieval of aerosol optical properties from Sun and sky radiance measurements. Journal of Geophysical Research: Atmospheres, 105(D16), 20673-20696.

Dumka, U., N. Tripathi, S., Misra, A., Giles, D., Eck, T., Sagar, R., & Holben, B. (2014). Latitudinal variation of aerosol properties from Indo-Gangetic plain to central Himalayan foothills during TIGERZ campaign. Journal of Geophysical Research: Atmospheres, 119(8), 4750-4769.

Goudie, A., & Middleton, N. (2001). Saharan dust storms: nature and consequences. Earth-science reviews, 56(1-4), 179-204.

Hamzeh, N. H., Kaskaoutis, D. G., Rashki, A., & Mohammadpour, K. (2021). Long-Term Variability of Dust Events in Southwestern Iran and Its Relationship with the Drought. Atmosphere, 12(10), 1350.

Holben, B. N., Eck, T. F., Slutsker, I. a., Tanre, D., Buis, J., Setzer, A., Vermote, E., Reagan, J. A., Kaufman, Y., & Nakajima, T. (1998). AERONET—A federated instrument network and data archive for aerosol characterization. Remote sensing of environment, 66(1), 1-16.

Hsu, N. C., Tsay, S.-C., King, M. D., & Herman, J. R. (2004). Aerosol properties over bright-reflecting source regions. IEEE Transactions on Geoscience and Remote Sensing, 42(3), 557-569.

Javadnia, E., & Abkar, A. A. (2017). Effect of Dust Storm on Optical and Radiative Properties of Aerosols Over Middle East [Research]. Journal of Geomatics Science and Technology, 7(1), 157-173.

Javadnia, E., Abkar, A. A., & Schubert, P. (2017). A MODIS-based modeling scheme for the estimation of downward surface shortwave radiation under cloud-free conditions. Arabian Journal of Geosciences, 10(17), 392.

Kaufman, Y., Tanré, D., Remer, L. A., Vermote, E., Chu, A., & Holben, B. (1997). Operational remote sensing of tropospheric aerosol over land from EOS moderate resolution imaging spectroradiometer. Journal of Geophysical Research: Atmospheres, 102(D14), 17051-17067.

Kutiel, H., & Furman, H. (2003). Dust storms in the Middle East: sources of origin and their temporal characteristics. Indoor and Built Environment, 12(6), 419-426.

Levelt, P. F., van den Oord, G. H., Dobber, M. R., Malkki, A., Visser, H., de Vries, J., Stammes, P., Lundell, J. O., & Saari, H. (2006). The ozone monitoring instrument. IEEE Transactions on geoscience and remote sensing, 44(5), 1093-1101.

Maleki, H., Sorooshian, A., Goudarzi, G., Nikfal, A., & Baneshi, M. M. (2016). Temporal profile of PM10 and associated health effects in one of the most polluted cities of the world (Ahvaz, Iran) between 2009 and 2014. Aeolian research, 22, 135-140.

Middleton, N. (1986). Dust storms in the Middle East. Journal of Arid Environments, 10(2), 83-96.

Miller, R., Perlwitz, J., & Tegen, I. (2004). Feedback upon dust emission by dust radiative forcing through the planetary boundary layer. Journal of Geophysical Research: Atmospheres, 109(D24).

More, S., Kumar, P., Gupta, P., Devara, P., & Aher, G. (2013). Comparison of aerosol products retrieved from AERONET, MICROTOPS and MODIS over a tropical urban city, Pune, India.

NASA Earth Observatory Natural Hazards. (2012). Dust storm in the Middle East. https://earthobservatory.nasa.gov/images/event/77454/dust-storm-in-the-middle-east

Nickovic, S., Kallos, G., Papadopoulos, A., & Kakaliagou, O. (2001). A model for prediction of desert dust cycle in the atmosphere. Journal of Geophysical Research: Atmospheres, 106(D16), 18113-18129.

Papi, R., Kakroodi, A., Soleimani, M., Karami, L., Amiri, F., & Alavipanah, S. K. (2022). Identifying sand and dust storm sources using spatial-temporal analysis of remote sensing data in Central Iran. Ecological Informatics, 70, 101724.

Prakash, P. J., Stenchikov, G., Kalenderski, S., Osipov, S., & Bangalath, H. (2014). The impact of dust storms on the Arabian Peninsula and the Red Sea. Atmospheric Chemistry & Physics Discussions, 14(13).

Rolph, G., Stein, A., & Stunder, B. (2017). Real-time environmental applications and display system: READY. Environmental Modelling & Software, 95, 210-228.

Sassen, K. (1991). The polarization lidar technique for cloud research: A review and current assessment. Bulletin of the American Meteorological Society, 72(12), 1848-1866.

Shahsavani, A., Naddafi, K., Haghighifard, N. J., Mesdaghinia, A., Yunesian, M., Nabizadeh, R., Arahami, M., Sowlat, M., Yarahmadi, M., & Saki, H. (2012). The evaluation of PM10, PM2. 5, and PM1 concentrations during the Middle Eastern Dust (MED) events in Ahvaz, Iran, from april through september 2010. Journal of arid environments, 77, 72-83.

Shahsavani, A., Yarahmadi, M., Jafarzade Haghighifard, N., Naimabadie, A., Mahmoudian, M. H., Saki, H., Sowlat, M. H., Soleimani, Z., & Naddafi, K. (2011). Dust Storms: Environmental and Health impacts [Review Article]. Journal of North Khorasan University of Medical Sciences, 2(4), 45-56.

Smirnov, A., Holben, B. N., Dubovik, O., O'Neill, N. T., Eck, T. F., Westphal, D. L., Goroch, A. K., Pietras, C., & Slutsker, I. (2002). Atmospheric aerosol optical properties in the Persian Gulf. Journal of the atmospheric sciences, 59(3), 620-634.

Soleimany, A., Solgi, E., Ashrafi, K., Jafari, R., & Grubliauskas, R. (2022). Investigating the performance of dust detection indices using MODIS data and products (Case study: Khuzestan province of Iran). Meteorology and Atmospheric Physics, 134(4), 1-14.

Velayatzadeh, M. (2020). Air pollution sources in Ahvaz city from Iran. Journal of Air Pollution and Health, 5(2), 147-152.

Wang, J., Xia, X., Wang, P., & Christopher, S. A. (2004). Diurnal variability of dust aerosol optical thickness and Angström exponent over dust source regions in China. Geophysical research letters, 31(8).

Winker, D., Vaughan, M., & Hunt, B. (2006). The CALIPSO mission and initial results from CALIOP. Lidar remote sensing for environmental monitoring VII, International Society for Optics and Photonics.